Selective epitaxial growth of AlGaAs/GaAs heterostructures on 300 mm Si(001) for red optical emission

Marie-Leonor Touraton, Mickael Martin, Sylvain David, Nicolas Bernier, Nevine Rochat, Jeremy Moeyaert, Virginie Loup, Frederic Boeuf, Christophe Jany, Didier Dutartre, et al.

► To cite this version:

Marie-Leonor Touraton, Mickael Martin, Sylvain David, Nicolas Bernier, Nevine Rochat, et al.. Selective epitaxial growth of AlGaAs/GaAs heterostructures on 300 mm Si(001) for red optical emission. Thin Solid Films, 2021, 721, pp.138541. 10.1016/j.tsf.2021.138541 . hal-03867639

HAL Id: hal-03867639

https://hal.univ-grenoble-alpes.fr/hal-03867639v1

Submitted on 22 Mar 2023

HAL is a multi-disciplinary open access archive for the deposit and dissemination of scientific research documents, whether they are published or not. The documents may come from teaching and research institutions in France or abroad, or from public or private research centers.

L'archive ouverte pluridisciplinaire **HAL**, est destinée au dépôt et à la diffusion de documents scientifiques de niveau recherche, publiés ou non, émanant des établissements d'enseignement et de recherche français ou étrangers, des laboratoires publics ou privés.

Distributed under a Creative Commons Attribution - NonCommercial 4.0 International License

Version of Record: https://www.sciencedirect.com/science/article/pii/S0040609021000249
Manuscript_684e21d55e8db0d8e45aed2fc3688359

Selective epitaxial growth of AlGaAs/GaAs heterostructures on 300 mm Si(001) for red optical emission

Marie-Leonor Touraton[a,b,c], Mickael Martin[b], Sylvain David[b], Nicolas Bernier[c], Nevine Rochat[c], Jeremy Moeyaert[b], Virginie Loup[c], Frederic Boeuf[a], Christophe Jany[c], Didier Dutartre[a], Thierry Baron[b,*]

[a] *STMicroelectronics, 850 rue Jean Monnet, F-38926 Crolles Cedex, France*
[b] *Univ. Grenoble Alpes, CNRS, CEA/LETI Minatec, LTM, F-38054 Grenoble Cedex, France*
[c] *Univ. Grenoble Alpes, CEA, LETI, Minatec Campus F-38054 Grenoble Cedex, France*

Abstract

Metal organic chemical vapor deposition of AlGaAs on GaAs on nominal 300 mm (001) Si was studied using selective epitaxial growth. Growth and structural characterization of AlGaAs layers formed on GaAs structures is presented. AlGaAs layers with different chemical compositions were fabricated on top of GaAs faceted structures. Energy Dispersive X-ray spectra were investigated to characterize the structure. It was found that the selective growth of AlGaAs structures for red optical emission needs careful temperature tuning. Indeed, AlGaAs layers show steep compositional variations depending on the crystallographic planes they are grown upon. Cathodoluminescence revealed that quantum well emission is best for the simpler rectangular shaped underlying GaAs structure. Thus, the obtained layers show that they could be excellent candidates for future red optical emitters directly integrated on a silicon wafer platform.

Keywords: Gallium arsenide, Aluminum gallium arsenide, Heterostructure, Selective Epitaxy, Metal-organic chemical vapor deposition

---

*Corresponding author
Email address: thierry.baron@cea.fr (Thierry Baron)

Preprint submitted to Thin Solid Films *January 10, 2021*

© 2021 published by Elsevier. This manuscript is made available under the CC BY NC user license
https://creativecommons.org/licenses/by-nc/4.0/

1. Introduction

Direct integration of III-V materials onto silicon substrates is currently seen as the best route for achieving low cost and sustainable optoelectronic devices. Indeed, the integration of an efficient light source directly onto silicon provides the possibility of a direct connection to the underlying silicon circuitry allowing high-functionality, increased-scalability and low-cost photonic integrated circuits. Most of the sources demonstrated today lie in the infrared region over 1150 nm [1, 2, 3] where silicon is transparent which minimizes propagation losses. Indeed, those sources are optically coupled to the silicon circuitry. Yet, there are other wavelengths of interest for emitters directly integrated on silicon. For instance, red sources are of use in emitters for display applications but also in silicon photonic lab-on-chip technologies targeting the life science market. However, for sources beneath 1150 nm there would be no optical coupling to the silicon circuitry. Direct integration of such a source on silicon would allow a low-cost chip to be made at a reduced material budget.

In order to make red laser diodes several optimizations were reported in literature over the years. The first visible light emitting diodes (LEDs) were made out of gallium arsenide phosphide, GaAsP, grown on top of gallium arsenide (GaAs) wafers. However, due to the large lattice mismatch with GaAs lots of defects were added to the layers. This is a non-existent concern with aluminum gallium arsenide (AlGaAs) as it is almost completely matched to GaAs. Hence, AlGaAs double heterostructures were used [4]. Further on, AlGaAs and GaAs single quantum well structures were used [5]. Then, AlGaAs and GaAs multiple quantum well structures were grown [6]. Nowadays, quaternary alloys as aluminum gallium indium phosphide, AlInGaP, [7, 8] are used which allows for a bandgap tuning while, being lattice matched to the substrate. However, due to the use of selective epitaxial growth, the use of quaternary alloys is challenging, which is why the GaAs/AlGaAs structure was chosen for the scope of this study. However, GaAs and AlGaAs materials exhibit a large lattice mismatch and a highly contrasting thermal expansion coefficient and a polarity difference

with silicon. This makes integration on silicon challenging regarding not having too many structural defects in the layers. Following years of research on those materials, two of the challenges can be taken care of. The difference of thermal expansion coefficient happens to not be a problem under around 7 μm of deposited material [9]. Antiphase boundaries can be suppressed using a pretreatment of the silicon [10]. Yet, the dislocations challenge arising from the lattice mismatch is still a threat to the optical emission and further on to the lifetime of future devices [11]. Different techniques are used to reduce dislocations in the active part of the devices. For example, strained layer super-lattices and thermal cycle annealing have proven to be efficient at reducing the dislocation density [12, 13]. However, they are time consuming and have a higher supply cost as much more material has to be grown. In order to make the process scalable for industry process, Aspect Ratio Trapping (ART) technique has been gaining attraction in the past years. It has been demonstrated to provide high quality material by confining the defects inside the opening of the dielectric pattern, or on the sides of the epitaxy [14, 15, 16]. Accordingly, the top part has less defects which grants the possibility of creating a device. Besides, the first ART optically pumped strip nano-laser was demonstrated in 2015 [17], and since the end of 2017 more demonstrators are currently being shown [18, 3, 19]. Most of these studies are dedicated to infra-red emission for Telecom and Datacom applications and deal with InGaAs alloys. There are few studies concerning AlGaAs alloys selectively grown on Si substrates for red emission. For application purpose, it is mandatory to control the materials quality and composition obtained by selective epitaxial growth (SEG) inside cavities.

In this paper, we have studied the selective epitaxy of GaAs/AlGaAs multilayers by using ART method. The heterostructures are grown by Metal-organic Chemical Vapor deposition (MOCVD) on patterned nominal 300 mm silicon (001) substrates, allowing direct integration of red sources with reduced structural defects.

2. Experimental details

On a Si (001) substrate, a 180 nm thick SiO_2 mask was deposited by plasma enhanced chemical vapor deposition and stripe patterns of 300 nm wide and several microns in length were formed by conventional photolithography and plasma etching process. The lines lie along the $<110>$ direction. Then, a wet tetramethylammonium hydroxide (TMAH) solution etch was undergone by the wafers to reveal the {111} planes of the silicon at the bottom of the ridges. We will refer to them as V-grooves. The wafers were prepared by a 6 min long dipping in a diluted solution containing 25% TMAH at 80 °C. The obtained trenches are about 400 nm in depth. Lastly, before the growth a SiCoNi™process was executed for surface cleaning and desoxydation. The SiCoNi™process relies on a remote plasma which creates reactive by-product species. When in contact with silicon oxide these species react and form a thin solid layer on the surface of the substrate which is then removed by sublimation [20]. The SEG was later accomplished using an Applied Materials 300 mm MOCVD system. Figure 1 shows a descriptive diagram of the obtained strip structures. The used precursor gases are Tri-Methyl Gallium (TMGa), Tri-Methyl Aluminum (TMAl) and Tertiary-Butyl-Arsine (TBAs) as Ga, Al and As sources. During the GaAs wire growth, the flux of TBAs and TMGa remained at values of 3015 μmol.min^{-1} and 355 μmol.min^{-1} respectively. In order to make the vertical stack structure, a first GaAs layer was grown using a two-step process combining a low temperature nucleation layer followed by a high temperature layer of better structural quality. It allows to form different crystallographic planes on the GaAs ridge. Afterwards the AlGaAs quantum well (QW) structure was designed and grown to obtain a red emission around 650 nm and 700 nm. All samples were capped by a 20 nm GaAs layer to prevent oxidation on the AlGaAs underlying structure. It is to note that the samples and focused ion beam (FIB) made lamellae were kept under N_2 atmosphere to avoid unwanted air exposure.

The characterization of the composition uniformity in the AlGaAs layers was performed by Energy Dispersive X-ray spectroscopy (EDX) and Transmission

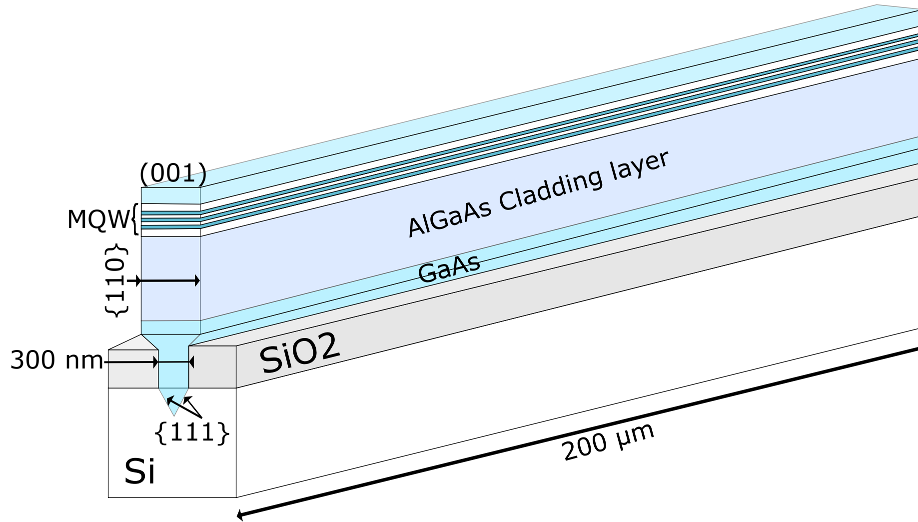

Figure 1: Descriptive diagram of the obtained ridge structures With the GaAs buffer, the AlGaAs cladding layer and the multiple quantum well (MQW) structure

90 Electron Microscopy (TEM) analysis on cross section lamellae. Lamellae were prepared inside a dual beam Focused Ion Beam-Scanning Electron Microscope, (FIB-SEM) Helios NanoLab 450S from FEI. The platinum layer was deposited on the samples in order to protect the patterns when slimming them down to achieve lamellae width of 130 nm. EDX analysis was performed at 200 kV 95 inside a FEI Tecnai TEM using an Oxford system. The High-Angular Annular Dark Field Scanning Transmission Electron Microscope (HAADF-STEM) image characterization was performed in a probe-corrected FEI Titan Themis STEM operated at 200 kV. Cathodoluminescence measurements were made at 10 K inside a Scanning Electron Microscope (SEM) with an acceleration tension of 5 100 keV. A CCD detector was used with an integration time per pixel of 1 ms. To extract the dislocation density a Gemini 500 ZEISS Field Emission Gun (FEG) SEM is used with an EDAX Hikari Super backscattered electron detector at 30 kV. The analysis was performed with this technique, referred to as Electron Channelling Contrast Imagery (ECCI), on a typical area of 1.8×10^{-7} cm^2.

105 ## 3. Results and discussion

The composition of the $Al_xGa_{1-x}As/Al_yGa_{1-y}As$ heterostructure was simulated in 2D with RSoft-LaserMOD software to obtain red emission. The Al composition of the barriers, cladding layer and quantum wells were calculated to be 45% and 30% respectively. The Al compositions were calculated to be 45%
110 for the barriers and cladding layers and 30% for the quantum wells. The thickness and composition of the bottom cladding layer is estimated to be 400 nm to avoid the optical losses in the underlying GaAs buffer and silicon substrate as well. The ideal structure is presented in Figure 1.

The growth of this structure by SEG-ART has been studied. To reduce
115 the structural defects density [21] in the active part of the device, a 400 nm GaAs buffer layer is grown inside the SiO_2 cavity before the growth of the AlGaAs cladding layer and multiple quantum wells out of the cavity. To avoid air exposure of Al containing layers, a GaAs capping was deposited at the top of the vertical structure. The relevant growth parameters for this study are
120 reported in Table 1 and have been calibrated on blanket wafers to match the right composition.

The typical ART process starts with the direct growth of a GaAs layer on the Si {111} planes using a standard two steps process: low temperature (LT) and high temperature (HT) [21]. The growth temperature, T_{growth}, for the HT
125 step has been varied from 600 °C to 650 °C. Figure 2 presents cross-sections of samples A1 and B1 after the complete heterostructure growth. If we focus solely on the GaAs buffer layer, the impact of T_{growth} on the GaAs shape is obvious. For A1 sample (600 °C), presented in Figure 2(a), a rectangular GaAs buffer made of one (001) top plane and two {110} facets at the sidewalls is formed. For
130 B1 sample (650 °C), shown in Figure 2(b), a pyramidal GaAs buffer made of two {111} and two {110} facets is obtained. A third shape called nailhead structure, sample C2, is formed as growth proceeds at 650 °C but with a shorter growth time than samples from series B. This growth temperature effect on morphology during SEG has already been documented in literature [22, 23]. We wanted to

Table 1: Summary of the different grown samples

Series	Sample number	Obtained facets on GaAs ridge	GaAs, T_{growth} [°C]	TMAl flux for barriers and cladding [μmol.min^{-1}]	TMAl flux for QWs [μmol.min^{-1}]
A	1	(001) & {110}	600	12	7.8
	2			24	15.6
B	1	{110} & {111}	650	12	7.8
	2			24	15.6
C	2	(001) & {110} & {111}		24	15.6

point out the fact that for device purpose, the rectangular shape with a flat top surface is desirable for the growth of QWs.

Then, the impact of these shapes on the growth of the AlGaAs heterostructures is evaluated. The cross-sections STEM view of a FIB-SEM prepared lamellae are shown on Figure 2(a) and Figure 2(b) and on Figure 3. Each GaAs buffer appears as the darker region in the image. We will now show that the cladding layer (between the GaAs buffer and the QWs) properties grown with the same conditions depends strongly on the shape of the GaAs buffers. At a first order, different zones labeled 2, 3, 4, corresponding to AlGaAs growth on various facets, namely (001), {110}, {111}, present different Al contents. The various grey levels seen in these figures can be associated with various degrees of Al content, as STEM is sensitive to the atomic weight. As Al is a light element the lighter the grey level, using a bright-field detector, the more Al incorporation there is in the AlGaAs layer. A strong dependence of Al incorporation with the crystalline nature of facets is demonstrated.

Furthermore, the chemical composition of each zone has been analyzed by

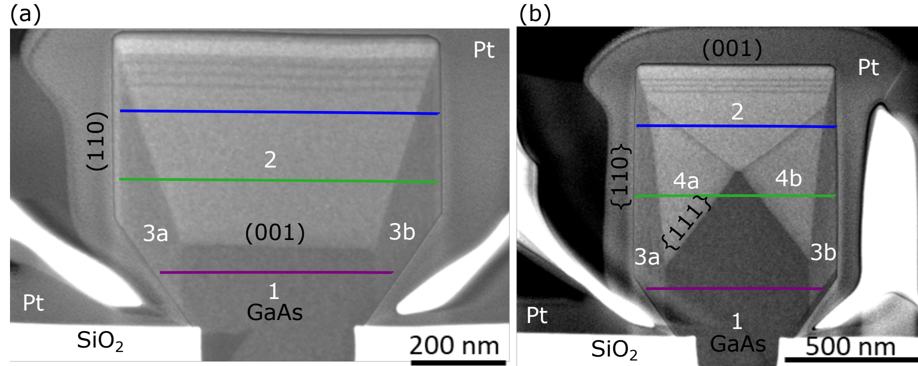

Figure 2: Cross-sectional Brigth-Field STEM images of the GaAs/AlGaAs ridge perpendicular to the ridge's direction showing three AlGaAs QWs embedded inside an AlGaAs matrix with GaAs grown at (a) 600 °C for sample A1 and (b) 650 °C for sample B1. The different zones of Al incorporation are indicated with numbers ranging from 1 to 4b. The three colour lines show where the EDX profiles where realized.

EDX. Linear profiles have been extracted at three different vertical positions corresponding approximately to the bottom, the middle and the top of the cladding layers. As a typical example, Figure 3 presents the chemical profiles on three different lines along the cross-section of sample C2.

155 At the basis of the nailhead, labeled 1 in Figure 3(a), the AlGaAs growth occurred on the {110} facets and reached a uniform composition of about 15%. From the second profile, (green line), we notice two distinct regions with an Al composition of 25% (zones 4a and 4b) and 15% (zones 3a and 3b) as growth proceeds on {111} and (001) facets respectively. The zones have symmetrical
160 percentages of Al along the center of the ridge. Two zones (2 and 3) remain at the top of the cladding layer with a composition of 15% and 25%. The intermediate region labeled 4 has disappeared.

The Al content for the different zone and each GaAs buffer shapes are summarized in Table 2.

165 While considering all the geometries (flat, pyramidal, nailhead), the Al incorporation remains constant for a dedicated facet and the same AlGaAs growth conditions. In samples A2, B2 and C2 zone 2 has a 26% Al content, zones 3a

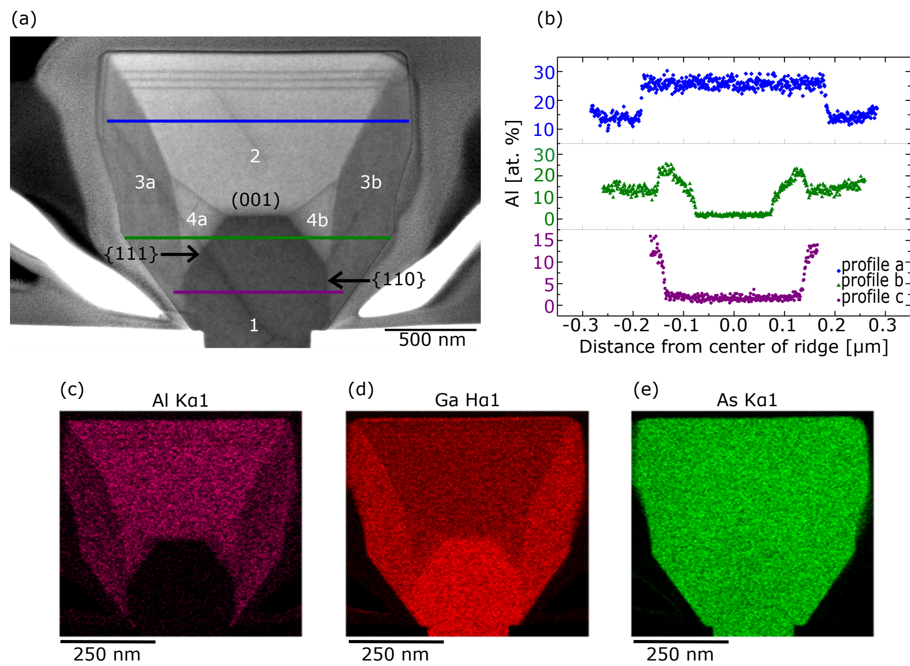

Figure 3: (a) Cross-sectional HAADF-STEM image of sample C2 the different zones of Al incorporation are indicated with numbers ranging from 1 to 4b. (b) EDX profiles of Al in sample C1. (c), (d) and (e) EDX mapping of Al, Ga and As elements in the sample.

Table 2: Summary of Al incorporation inside the different zones

Series	Sample number	Al [at. %] in zone					
		1	2 (001)	3a {110}	3b {110}	4a {111}	4b {111}
A	1	1.8 +/- 0.1	14.0 +/- 0.9	7.4 +/- 1.6	7.7 +/- 1.1	No {111} facets	
	2	1.8 +/- 0.2	26.2 +/- 0.4	13.0 +/- 1.9	13.1 +/- 2.3		
B	1	1.6 +/- 0.2	14.1 +/- 0.4	7.5 +/- 0.7	7.0 +/- 0.9	12.7 +/- 1.5	13.0 +/- 0.3
	2	1.7 +/- 0.5	26.6 +/- 1.2	14.2 +/- 1.9	14.3 +/- 1.4	18.5 +/- 3.1	22.2 +/- 3.7
C	2	1.8 +/- 0.1	25.8 +/- 0.1	13.5 +/- 0.2	13.3 +/- 1.3	17.6 +/- 0.6	15.8 +/- 1.1

and 3b contain 14% Al. Samples B2 and C2 exhibit two supplementary zones, 4a and 4b containing around 20% Al. In regards to sample A1 and B1 zone 2 holds a 14% incorporation of Al and zones 3a and 3b include 7% Al.

From Figure 2 and Figure 3, the AlGaAs growth rate on the different facets can be extracted. For samples A1 and B1 the growth rates are respectively 1.1 nm/s along the (001) plane and 0.3 nm/s along the {110} planes. For B2 sample, the growth along the {111} planes is 1.2 nm/s. For samples A2, B2 and C2, the growth rates remain the same for the growth upon planes (001) and {111} and doubles to 0.6 nm/s for the growth upon {110} planes. Therefore, with a doubled TMAl precursor flux, the lateral expansion of the ridge is favored. A summary of the different growth rates is presented in Table 3.

For all the samples, the growth rates are from highest to lowest obtained in the following order $\{111\} > (001) > > \{110\}$. From Table 2, the Al incorporation is from highest to lowest grown upon the following facets $(001) > \{111\} > \{110\}$. It is possible to notice that for samples with number 2, the aluminum

Table 3: Summary of the AlGaAs layers growth rate upon the various facets.

<table>
<tr><th rowspan="2">Series</th><th rowspan="2">Sample number</th><th colspan="3">Growth rate [nm/s]</th></tr>
<tr><th>Zone 2 (001)</th><th>Zone 3 {110}</th><th>Zone 4 {111}</th></tr>
<tr><td rowspan="2">A</td><td>1</td><td rowspan="5">1.1</td><td>0.3</td><td rowspan="2">No {111} facets</td></tr>
<tr><td>2</td><td>0.6</td></tr>
<tr><td rowspan="2">B</td><td>1</td><td>0.3</td><td rowspan="3">1.2</td></tr>
<tr><td>2</td><td rowspan="2">0.6</td></tr>
<tr><td>C</td><td>2</td></tr>
</table>

incorporation in each zone is approximately doubled compared to the same zone in samples with number 1, which is consistent with the increase of the TMAl flux. From these observations, it is not easy to correlate the growth rate with the incorporation of Al in the different zones as it was previously shown for In incorporation in $In_xGa_{1-x}As$ alloys grown on different orientations by Elsner et al. [24]. Indeed, here when doubling the TMAl flow in the chamber an enhanced Al incorporation is observed on facets (001) and {111} however, the growth rates on those facets remains identical.

However, similar findings to our structures were also shown by Borg et al. They report the growth of InGaAs horizontal structures using Template Assisted Selective Epitaxy (TASE) [25]. Their structures were grown inside a horizontal template having the same shape as our finished structures. Their structures exhibit two compositional regions comparable to our series A samples. Due to their use of TASE templates the main mechanism explaining the incorporation differences are reaction limited. This allows to govern the growth by a facet-dependent chemical reaction [25]. In our case we should not be limited by chemical rate but rather by mass transport as our AlGaAs growth occurs outside the patterned trenches hence, entering in a regime where one should start exhibiting similar growth as on planar substrates. Nonetheless, we also seem to be in the limited reaction regime. Indeed, similar structures

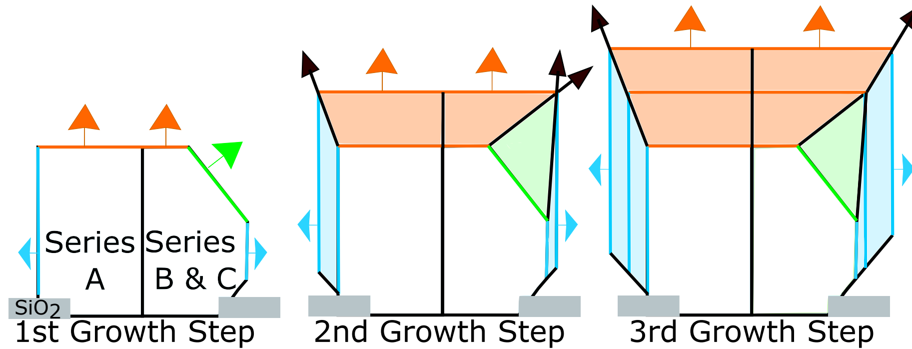

Figure 4: Schematic illustration in three growth steps of the combined growth on the various facets leading to the final compositional structure. The left hand-sight represents samples from series A the right hand-sight samples from series B and C. The growth upon facets (001), {110} and {111} are shown in orange, blue and green.

grown on non-planar substrates exhibiting compositional variations depending on the crystallographic planes they are grown upon were presented by Biasiol and Kapon [26]. They referred to them as "self-limiting" due to the appearance of a growth front in between the various compositions. Their self-limiting evolution depends on growth rate anisotropy exhibited on the different facets and capillarity induced diffusion. Here, we observe that the different growth rates that we have on the various facets plays a critical role. We will also show that we exhibit capillarity induced diffusion.

Schematic scenarios for the growth of AlGaAs on the different shaped GaAs buffer layers are drawn in Figure 4. Faster growth rate upon {111} facets always leads to its disappearance, leaving room for growth only on (001) and {110} facets. A similar effect was depicted for silicon SEG at high temperatures [27]. The zone grown on the (001) facet allows for a smooth integration of quantum wells at the top of the structure with desired composition for red emission. The impact of the heterostructures grown on the {110} facets has to be evaluated.

Sample A2, as a representative example, has been characterized by HRSTEM to carefully examine the transition between the alloys grown on {110} facets and (001) plane.

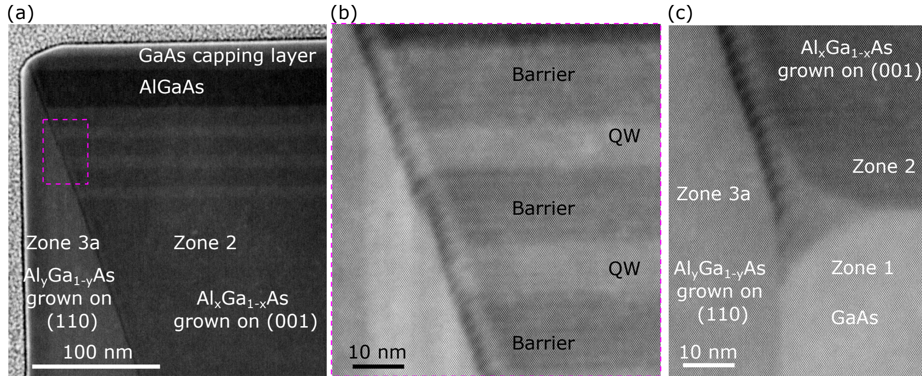

Figure 5: (a) TEM microscopy of the interface zone on sample A2. (b) TEM microscopy of the interface zone on sample A2 zoomed on the QW zone. (c) Concave faceting of GaAs stud.

Figure 5(a) presents the QWs and cladding regions where a clear and abrupt separation between zone 2 and 3a can be observed. From the zoom shown in figure 5(b), on can see a very dark contrast at the growth front in between zones 2 and 3a. A closer look can be taken by paying closer attention at the transition between the GaAs buffer and the cladding layer, where growth starts both on (001) and {111} planes as displayed in figure 5(c). Actually, one can see a curved GaAs structure where one could expect an edge in between (001) and {111} facets. On each side of the curvature the two zones 2 and 3a can be well identified. Added to that, one can recognize the very dark contrast at the growth front and notice that it starts close to the curvature of the GaAs. This almost black contrast can be attributed to a fluctuation of Al content.

This singularity was also documented in corner-overgrown GaAs/AlGaAs core-shell nanowires [28, 29]. It was associated with curvature-induced capillarity effects, leading to ternary alloy segregation and hence allowing aluminum fluctuation [30, 31]. In our case segregation of aluminum from high Al-content to low Al-content zone could explain this effect. Indeed, from Biasol and Kapon's paper [26] the non-uniform profile of the chemical profile and the strong bonds exhibited by Al towards As compared to Ga bonds to As boosts Al incorporation at the convex edges. Therefore, we can safely assume that the specific

240 growth we obtain can be explained solely by the growth rate anisotropy and the capillarity induced effects on the convex edges.

To investigate the impact of the various Al incorporation in function of the GaAs shaped buffer, cathodoluminescence (CL) experiments were made at 10 K in cross-section and in top-view.

245 Figure 6(c) shows a 10 K panchromatic CL mapping of B1 sample taken in cross-section. The quantum wells emission is centered around 690 nm +/- 5 nm as displayed in green. In contrast the barriers emit around 664 nm +/- 10 nm as shown in blue in figure 6(b), and the AlGaAs cladding layer emitting between 800 nm and 850 nm as shown in red in figure 6(a). The barriers and cladding 250 layers have a five to six times lower intensity as compared to the quantum wells. The same type of measurements has been done on the other samples and they exhibit the same characteristics.

In regards to the A1 sample, shown in Figure 6(d), the contribution from the GaAs is very low which is attributed to the geometry of Al incorporation inside 255 the structure. One can find similar contributions as the one seen in B1 sample. Quantum wells emit around 700 nm +/- 5 nm, the underlying AlGaAs region emits between 760 nm and 825 nm. The barriers have an emission around 675 nm +/- 10 nm.

For both samples the emission from the quantum wells and the barriers are 260 localized at the center of the ridge. As shown in Figure 5(b), the quantum wells curvature observed between zone 2 and 3 allows to have a particularly well confined emission zone on the center part of the structure. This phenomenon has already been reported by Kunert et al. [14].

However, the signal intensity is much higher in sample A1 than in sample 265 B1. From this, it is then possible to see that the underlying morphology of the samples seems to play a key role in the optical response of the structure. Therefore, it is of utmost importance to understand how the facet growth happens in order to get the best emitting structure for a future integration.

As Figure 6(d) shows a 10 K panchromatic CL cross-section mapping of 270 quantum wells contribution in sample A1, Figure 7(b) displays the quantum

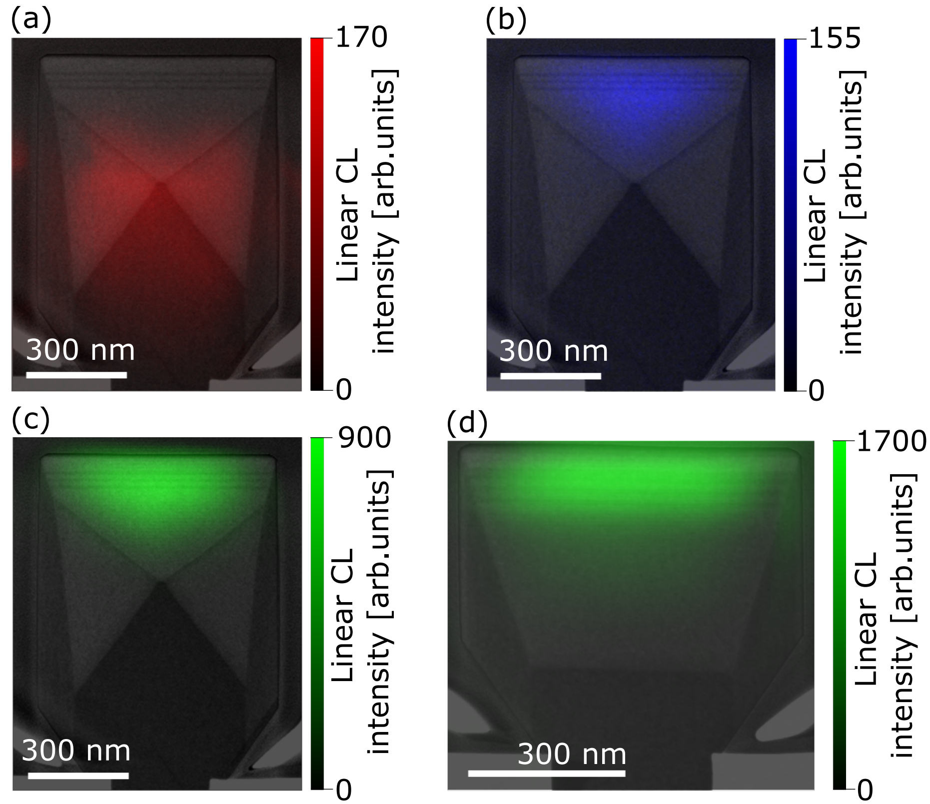

Figure 6: 10 K panchromatic CL mapping superposed to the FIB-SEM cross-section to visualize the different contributions. (a) GaAs and low containing Al in the AlGaAs layers between 800 and 850 nm for sample B1. (b) Barriers contribution at 664 nm for sample B1. (c) QWs contribution at 690 nm for sample B1. (d) QWs contribution at 700 nm for sample A1.

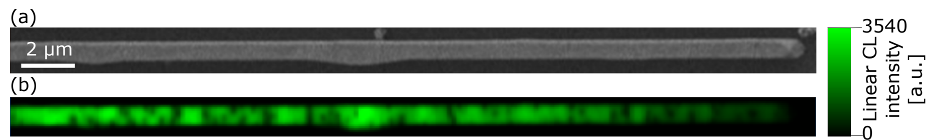

Figure 7: (a) Top-view SEM image of the mapped ridge. (b) 10 K panchromatic CL mapping of quantum wells, at 700 nm, contribution in sample A1.

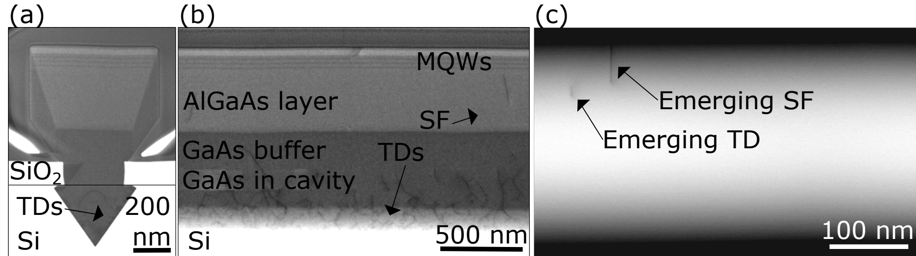

Figure 8: (a) Cross-sectional SEM image of the A1 GaAs/AlGaAs ridge perpendicular to the ridge's direction. The limit between the dielectric and the silicon is shown by a horizontal dark line. (b) Cross-sectional STEM image of the A1 GaAs/AlGaAs ridge along the <110> direction. (c) ECC top View of a section of A2 ridge.

wells emission from a top-view point for this same sample. Figure 7 shows a very high intensity emission from the quantum wells of sample A1. Indeed, for the same integration time with the same conditions B1 sample has 4 times less signal than A1 sample.

275 CL taken in top view reveals the presence of dark spots which could be attributed to crystalline defects. Indeed, although ART method has been used to prevent the propagation of defects outside of the cavities, the aspect ratio height of our sample's cavities is 0.35 whereas, a value above 1.43 is required to be really effective [32]. Accordingly, some defects should still propagate to 280 the top part of the structure. A defect analysis was then performed to see if the registered number of dark spots could be connected to a measured defect density.

The presence of crystalline defects inside our heterostructures has been analyzed by SEM in cross section perpendicularly to the wire (Figure 8(a)) and 285 along the wire direction (Figure 8(b)). The images reveal that most of the dislocations are confined in the bottom part of the ridge. The top view image taken using a backscattered electron detector inside a SEM, allows to image existing defects at the surface by ECCI technique on a relevant total area of around 1.8×10^{-7} cm^2.

290 In a 2 μm long section only, one twin is observed and the defects density

beneath the quantum wells position is evaluated to be 2.8×10^8 cm^{-2}. Half of the defects are linear ones and the other half are planar ones. The total number of defects can also be accounted as a linear density, here 1.6 defects/μm. As a comparison, it is possible to observe around 42 extinction points in CL analyses for a 30 μm long wire. The linear density is hence 1.4 dark spots/μm which is consistent with the crystalline defect linear density. Thus, it highlights the importance of mastering the propagation of the defects to confine them in the trench part. Our results are consistent with the ones from Kunert's group [32] obtained for similar sized trenches.

4. Conclusions

We have presented an analysis of compositional variation in the case of selective growth of AlGaAs multilayers on GaAs using selective epitaxial growth inside V-groove SiO_2 ridges on (001) silicon 300 mm. We can acknowledge the specific type of growth depending on crystallographic orientation that happens with AlGaAs alloys using EDX measurements and TEM microscopy. We confirmed that our structures show higher Al incorporation upon the (001) facet. Moreover, the "self-limiting" growth phenomenon favors the expansion of the top facet. This allows a planar integration of quantum wells. We also demonstrated that the underlying morphology highly impacts the optical response. One needs to favor the simpler underlying structure. Indeed, by lessening the number of compositional areas the better the optical response of the structure is. We also emphasize the importance of decreasing the defect density as they hinder drastically the luminescence of parts of the sample. From all the above characterizations the rectangular shaped GaAs configuration, made of one (001) top plane and two {110} facets at the sidewalls, seems much more adapted for an optical emitter. Which would require adding a top AlGaAs cladding layer for the optical guiding. The results emphasize the promise of those aspect selective epitaxial grown structures for future optical emission on an integrated silicon platform.

Acknowledgments

This work was supported by the French "Recherches Technologiques de Base" (Basis Technological Research) and RENATECH programs and by the French government managed by ANR under the Investissements d'avenir economic stimulus package, with reference IRT Nanoelec ANR-10-IRT-05 and ANR-15-IDEX-02. The authors want to thank Franck Bassani for the helpful suggestions, the CEA-Leti clean room staff and Frederic Charlot from the CMTC platform in Grenoble.

References

[1] K. Li, Z. Liu, M. Tang, M. Liao, D. Kim, H. Deng, A. M. Sanchez, R. Beanland, M. Martin, T. Baron, S. Chen, J. Wu, A. Seeds, H. Liu, O-band InAs/GaAs quantum dot laser monolithically integrated on exact (001) Si substrate, Journal of Crystal Growth 511 (2019) 56–60. doi:10.1016/j.jcrysgro.2019.01.016.

[2] S. Chen, M. Liao, M. Tang, J. Wu, M. Martin, T. Baron, A. Seeds, H. Liu, Electrically pumped continuous-wave 1.3μm InAs/GaAs quantum dot lasers monolithically grown on on-axis Si (001) substrates, Optics Express 25 (5) (2017) 4632. doi:10.1364/oe.25.004632.

[3] B. Shi, S. Zhu, Q. Li, Y. Wan, E. L. Hu, K. M. Lau, Continuous-wave optically pumped 1.55 μm InAs/InAlGaAs quantum dot microdisk lasers epitaxially grown on silicon, ACS Photonics 4 (2) (2017) 204–210. doi:10.1021/acsphotonics.6b00731.

[4] S. Yamamoto, H. Hayashi, T. Hayakawa, N. Miyauchi, S. Yano, T. Hijikata, Room-temperature cw operation in the visible spectral range of 680–700 nm by AlGaAs double heterojunction lasers, Applied Physics Letters 41 (9) (1982) 796–798. doi:10.1063/1.93691.

[5] T. Hayakawa, K. Takahashi, T. Suyama, M. Kondo, S. Yamamoto, T. Hijikata, High reliability in AlGaAs laser diodes prepared by molecular beam epitaxy on 0.5°-misoriented (111)B substrates, Japanese Journal of Applied Physics 27 (Part 2, No. 5) (1988) L889–L891. doi:10.1143/jjap.27.l889.

[6] T. Hayakawa, T. Suyama, K. Takahashi, M. Kondo, S. Yamamoto, T. Hijikata, Low-threshold room-temperature cw operation of $(\mathrm{AlGaAs})_m(\mathrm{GaAs})_n$ superlattice quantum well lasers emitting at ∼680 nm, Applied Physics Letters 51 (10) (1987) 707–709. doi:10.1063/1.98895.

[7] K. Streubel, U. Helin, V. Oskarsson, E. Backlin, A. Johansson, High brightness visible (660 nm) resonant-cavity light-emitting diode, IEEE Photonics Technology Letters 10 (12) (1998) 1685–1687. doi:10.1109/68.730469.

[8] C. Kaspari, M. Zorn, M. Weyers, G. Erbert, Growth parameter optimization of the GaInP/AlGaInP active zone of 635nm red laser diodes, Journal of Crystal Growth 310 (23) (2008) 5175–5177. doi:10.1016/j.jcrysgro.2008.07.018.

[9] V. K. Yang, M. Groenert, C. W. Leitz, A. J. Pitera, M. T. Currie, E. A. Fitzgerald, Crack formation in GaAs heteroepitaxial films on Si and SiGe virtual substrates, Journal of Applied Physics 93 (7) (2003) 3859–3865. doi:10.1063/1.1558963.

[10] R. Alcotte, M. Martin, J. Moeyaert, R. Cipro, S. David, F. Bassani, F. Ducroquet, Y. Bogumilowicz, E. Sanchez, Z. Ye, X. Y. Bao, J. B. Pin, T. Baron, Epitaxial growth of antiphase boundary free GaAs layer on 300 mm Si(001) substrate by metalorganic chemical vapour deposition with high mobility, APL Materials 4 (4) (2016) 046101. doi:10.1063/1.4945586.

[11] D. Jung, R. Herrick, J. Norman, K. Turnlund, C. Jan, K. Feng, A. C. Gossard, J. E. Bowers, Impact of threading dislocation density on the lifetime of InAs quantum dot lasers on Si, Applied Physics Letters 112 (15) (2018) 153507. doi:10.1063/1.5026147.

375 [12] M. Tang, S. Chen, J. Wu, Q. Jiang, V. G. Dorogan, M. Benamara, Y. I. Mazur, G. J. Salamo, A. Seeds, H. Liu, 1.3μm InAs/GaAs quantum-dot lasers monolithically grown on Si substrates using InAlAs/GaAs dislocation filter layers, Optics Express 22 (10) (2014) 11528. doi:10.1364/oe.22.011528.

380 [13] N. Hayafuji, M. Miyashita, T. Nishimura, K. Kadoiwa, H. Kumabe, T. Murotani, Effect of employing positions of thermal cyclic annealing and strained-layer superlattice on defect reduction in GaAs-on-si, Japanese Journal of Applied Physics 29 (Part 1, No. 11) (1990) 2371–2375. doi:10.1143/jjap.29.2371.

385 [14] B. Kunert, W. Guo, Y. Mols, B. Tian, Z. Wang, Y. Shi, D. V. Thourhout, M. Pantouvaki, J. V. Campenhout, R. Langer, K. Barla, III/V nano ridge structures for optical applications on patterned 300 mm silicon substrate, Applied Physics Letters 109 (9) (2016) 091101. doi:10.1063/1.4961936.

[15] L. Megalini, B. Bonef, B. C. Cabinian, H. Zhao, A. Taylor, J. S. Speck,
390 J. E. Bowers, J. Klamkin, 1550-nm InGaAsP multi-quantum-well structures selectively grown on v-groove-patterned SOI substrates, Applied Physics Letters 111 (3) (2017) 032105. doi:10.1063/1.4994318.

[16] Y. Li, M. Wang, X. Zhou, P. Wang, W. Yang, F. Meng, G. Luo, H. Yu, J. Pan, W. Wang, InGaAs/InP multi-quantum-well nanowires with a lower
395 optical leakage loss on v-groove-patterned SOI substrates, Optics Express 27 (2) (2019) 494. doi:10.1364/oe.27.000494.

[17] Z. Wang, A. Abbasi, U. Dave, A. D. Groote, S. Kumari, B. Kunert, C. Merckling, M. Pantouvaki, Y. Shi, B. Tian, K. V. Gasse, J. Verbist, R. Wang, W. Xie, J. Zhang, Y. Zhu, J. Bauwelinck, X. Yin, Z. Hens, J. V. Campen-
400 hout, B. Kuyken, R. Baets, G. Morthier, D. V. Thourhout, G. Roelkens, Novel light source integration approaches for silicon photonics, Laser & Photonics Reviews 11 (4) (2017) 1700063. doi:10.1002/lpor.201700063.

[18] Y. Han, W. K. Ng, C. Ma, Q. Li, S. Zhu, C. C. S. Chan, K. W. Ng, S. Lennon, R. A. Taylor, K. S. Wong, K. M. Lau, Room-temperature
405 InP/InGaAs nano-ridge lasers grown on si and emitting at telecom bands, Optica 5 (8) (2018) 918. doi:10.1364/optica.5.000918.

[19] Y. Han, W. K. Ng, Y. Xue, Q. Li, K. S. Wong, K. M. Lau, Telecom InP/InGaAs nanolaser array directly grown on (001) silicon-on-insulator, Optics Letters 44 (4) (2019) 767. doi:10.1364/ol.44.000767.

410 [20] P. Raynal, V. Loup, L. Vallier, M. Martin, J. Moeyaert, B. Pelissier, P. Rodriguez, J. Hartmann, P. Besson, Wet and Siconi® cleaning sequences for SiGe p-type metal oxide semiconductor channels, Microelectronic Engineering 187-188 (2018) 84 – 89. doi:10.1016/j.mee.2017.12.003.

[21] R. Cipro, T. Baron, M. Martin, J. Moeyaert, S. David, V. Gorbenko,
415 F. Bassani, Y. Bogumilowicz, J. P. Barnes, N. Rochat, V. Loup, C. Vizioz, N. Allouti, N. Chauvin, X. Y. Bao, Z. Ye, J. B. Pin, E. Sanchez, Low defect InGaAs quantum well selectively grown by metal organic chemical vapor deposition on Si(100) 300 mm wafers for next generation non planar devices, Applied Physics Letters 104 (26) (2014) 262103. doi:10.1063/1.4886404.

420 [22] E. Gil-Lafon, A. Trassoudaine, D. Castelluci, A. Pimpinelli, R. Saoudi, O. M. Parriaux, A. Muravaud, C. Darraud, Submicrometer scale growth morphology control: a new route for the making of photonic crystal structures?, in: C. Amra, N. Kaiser, H. A. Macleod (Eds.), Advances in Optical Thin Films, SPIE, 2004. doi:10.1117/12.513376.

425 [23] R. Cipro, Epitaxie en phase vapeur aux organométalliques et caractérisation de semi-conducteur III-As sur substrat silicium dans une plateforme microélectronique, Theses, Université Grenoble Alpes (Jun. 2016).
URL https://tel.archives-ouvertes.fr/tel-01390505

[24] B. Elsner, R. Westphalen, K. Heime, P. Balk, Deposition by LP-MOVPE in
430 the ga-in-as-p system on differently oriented substrates, Journal of Crystal Growth 124 (1-4) (1992) 326–332. doi:10.1016/0022-0248(92)90479-3.

[25] M. Borg, L. Gignac, J. Bruley, A. Malmgren, S. Sant, C. Convertino, M. D. Rossell, M. Sousa, C. Breslin, H. Riel, K. E. Moselund, H. Schmid, Facet-selective group-III incorporation in InGaAs template assisted selective epitaxy, Nanotechnology 30 (8) (2018) 084004. doi:10.1088/1361-6528/aaf547.

[26] G. Biasiol, E. Kapon, Mechanisms of self-ordering of quantum nanostructures grown on nonplanar surfaces, Physical Review Letters 81 (14) (1998) 2962–2965. doi:10.1103/physrevlett.81.2962.

[27] D. Dutartre, A. Talbot, N. Loubet, Facet propagation in si and SiGe epitaxy or etching, in: ECS Transactions, ECS, 2006. doi:10.1149/1.2355845.

[28] L. Steinke, P. Cantwell, D. Zakharov, E. Stach, N. J. Zaluzec, A. F. i Morral, M. Bichler, G. Abstreiter, M. Grayson, Nanometer-scale sharpness in corner-overgrown heterostructures, Applied Physics Letters 93 (19) (2008) 193117. doi:10.1063/1.2988526.

[29] L. Mancini, Y. Fontana, S. Conesa-Boj, I. Blum, F. Vurpillot, L. Francaviglia, E. Russo-Averchi, M. Heiss, J. Arbiol, A. F. i Morral, L. Rigutti, Three-dimensional nanoscale study of al segregation and quantum dot formation in GaAs/AlGaAs core-shell nanowires, Applied Physics Letters 105 (24) (2014) 243106. doi:10.1063/1.4904952.

[30] D. Rudolph, S. Funk, M. Döblinger, S. Morkötter, S. Hertenberger, L. Schweickert, J. Becker, S. Matich, M. Bichler, D. Spirkoska, I. Zardo, J. J. Finley, G. Abstreiter, G. Koblmüller, Spontaneous alloy composition ordering in GaAs-AlGaAs core–shell nanowires, Nano Letters 13 (4) (2013) 1522–1527. doi:10.1021/nl3046816.

[31] B. Loitsch, N. Jeon, M. Döblinger, J. Winnerl, E. Parzinger, S. Matich, U. Wurstbauer, H. Riedl, G. Abstreiter, J. J. Finley, L. J. Lauhon, G. Koblmüller, Suppression of alloy fluctuations in GaAs-AlGaAs core-shell nanowires, Applied Physics Letters 109 (9) (2016) 093105. doi:10.1063/1.4962269.

[32] B. Kunert, Y. Mols, M. Baryshniskova, N. Waldron, A. Schulze, R. Langer, How to control defect formation in monolithic III/v hetero-epitaxy on (100) si? a critical review on current approaches, Semiconductor Science and Technology 33 (9) (2018) 093002. doi:10.1088/1361-6641/aad655.